

## Multifragmentation and dynamics in heavy ion collisions

R ROY\*

Laboratoire de Physique Nucléaire, Département de Physique, Université Laval, Québec G1K 7P4, Canada

**Abstract.** A midrapidity zone formed in heavy-ion collisions has been investigated through special selections of light particles and intermediate mass fragments detected in the reaction  $^{35}\text{Cl}$  on  $^{12}\text{C}$  at 43 MeV/nucleon and the reactions  $^{58}\text{Ni}$  on  $^{12}\text{C}$ ,  $^{24}\text{Mg}$ , and  $^{197}\text{Au}$  at 34.5 MeV/nucleon, and of neutron energy spectra measured in the reaction  $^{35}\text{Cl}$  on  $^{nat}\text{Ta}$ . Properties of the observables have been examined to characterize the neck-like structure formed between the two reaction partners.

**Keywords.** Hot nuclei; multifragmentation; equilibrium; statistical emission; dynamics; neck emission.

**PACS Nos** 25.70.Lm; 25.70.Mn

### 1. Introduction

The investigation of heavy-ion collision mechanisms at intermediate energies, around the nucleon Fermi energy, have set major understanding objectives to reach. For several years, such studies have been focusing on intermediate-mass fragment (IMF) production. More specifically, the probing of nuclear liquid-gas phase transition and multifragmentation (MF) [1] have been important features of research programmes on properties of hot nuclei and their decay channels. Has equilibrium been reached before the disintegration stage? Timescale is proved to be crucial. The statistical emission picture is confronted to dynamical perspectives of several mechanism properties: where are the frontiers? How can we establish their own limits? A first significant experimental evidence of phase transition has been displayed through a caloric curve [2], but it was rapidly realized that some related steps were complex and had to be traced [3]. Other signs of phase transitions have been reported [4]. An important progress has been made as well in theoretical predictions as in experimental results.

In this paper, we report several works accomplished by the heavy ion group at Laval University. After a brief presentation (§2) of the multidetection array operated to perform the experiments, some experimental results from the reaction  $^{35}\text{Cl}$  on  $^{12}\text{C}$  (§3) will be

---

\*For the HERACLES collaboration.

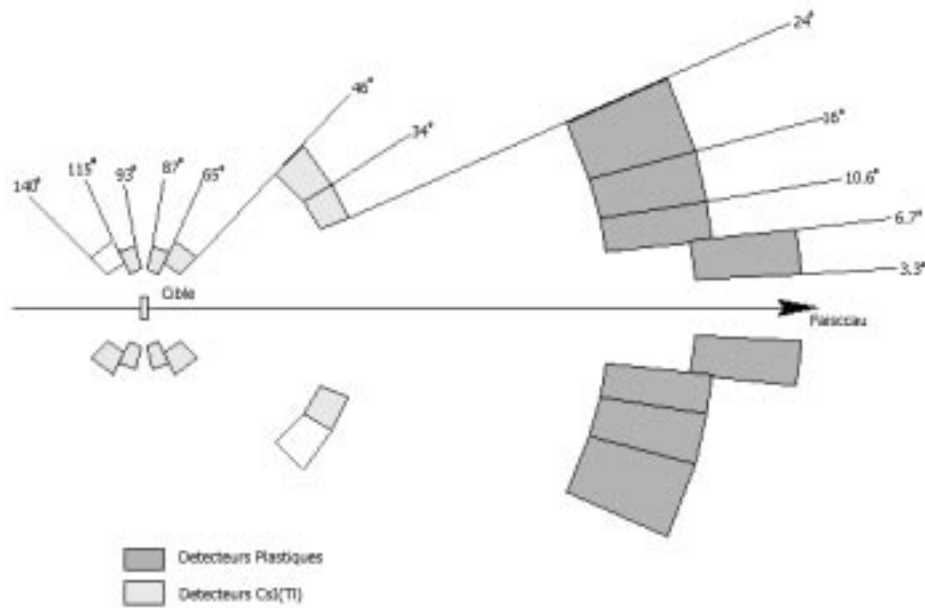


**Figure 1.** The Chalk River–Laval array. The beam comes from the left.

discussed to show the presence and properties of midrapidity emission generated through the formation of a neck-like structure, and its confirmation from neutron detection in the  $^{35}\text{Cl} + ^{\text{nat}}\text{Ta}$  reaction. Timescale measurements on the  $^{58}\text{Ni} + ^{197}\text{Au}$  reaction are discussed in the last section, along with an analysis stressing the important role of neutron asymmetry for the midrapidity emission. The report will be completed by a general conclusion.

## 2. Experimental facilities

All experimental results discussed in the present paper have been obtained from experiments performed at the Tandem Accelerator Superconducting Cyclotron (TASCC) facility of Chalk River Laboratories. Charged particles have been detected in the CRL–Laval (Chalk River Laboratories–Université Laval)  $4\pi$  multidetector array. In its most complete version (see figure 1), it is constituted of 144 detectors mounted in concentric rings covering polar angles between  $3.3^\circ$  and  $140^\circ$ . The array covers more than 80% of the solid angle around the target with ten rings of 12 to 16 modules each depending on the polar angle. The forward four rings, between  $3.3^\circ$  and  $24^\circ$ , are made of 16 plastic phoswich detectors; the energy thresholds are 7.5 (27.5) MeV/nucleon for element identification of  $Z = 1$  (28) particles. The remaining six rings are all made of CsI(Tl) scintillators achieving isotopic resolution for  $Z = 1, 2$  particles and charge identification up to  $Z = 4$ , with effective energy thresholds between 2 and 5 MeV/nucleon. In some given experiments, Si–CsI(Tl) or Si–Si–CsI(Tl) telescopes are added at different places in the multidetector so that isotopic

resolution can be achieved for heavier nuclei, according to the experiment requirements. More detailed specifications and modi operandi can be found elsewhere [4,6].

### **3. Evidence of a neck-like formation**

The formation of a neck-like structure has been evidenced between very heavy ions with a projectile in the Fermi energy range [5]. This phenomenon is not well understood. To study collisions between light heavy ions, the  $^{35}\text{Cl}$  projectile on a  $^{12}\text{C}$  target has been used to look for midrapidity emission. The array was mounted with the five regular concentric rings from  $6.8^\circ$  to  $46.8^\circ$  (see figure 1), three Si–CsI(Tl) telescopes being added at the most forward angles,  $3^\circ$ – $5^\circ$ . Performed at 43 MeV/nucleon, the experiment has given rise to different types of analysis [6]. Evidence of a neck-like structure has been established from analysing charged particles emitted at velocities between those characteristic of projectilelike (PLE) and target-like (TLE) emitters.

A first selection is made on the data set (events with total charge detected,  $\Sigma Z = 23$ ) by requiring that the flow angle be larger than  $45^\circ$ ; that cut is performed with the quadratic momentum tensor [7] which allows the determination of the major axis of the event in momentum space. The angle between that axis and the beam axis is the flow angle of an event. By doing so, events with binary, or ternary, nature are privileged, because a neck-like structure is most likely to appear in those events. Since a parallel velocity distribution of particles with  $2 \leq Z \leq 9$  coincident with a projectile-like fragment shows a three-peak structure [6], rather than a sum of a pure fusion (one-source) component added to a binary one, an exclusive analysis has been based on the heaviest particle of each event. Moreover, two-source filtered simulations from EUGENE [8] show that particles from TLE are mostly detected by CsI(Tl) scintillators (from  $24^\circ$  to  $47^\circ$ ), whereas PLE particles are in the Si–CsI telescopes and phoswich detectors (from  $3^\circ$  to  $24^\circ$ ). In consequence, the results of figures 2 and 3 have been collected, event by event, to probe the origin of charged particles. The two ‘forward’ heaviest particles and the heaviest one emitted ‘backward’ in the center-of-mass (c.m.) frame were identified for each event; their individual and total distributions are presented in figure 2. The forward heaviest CP(2–9) has an average velocity of 1.7 cm/ns and the second one has a major contribution near the c.m. velocity at  $-1.5$  cm/ns. The panel (d) shows a smooth distribution from  $-4$  to  $+4$  cm/ns. Figure 3 displays the same velocity distributions, but for the filtered EUGENE two-source simulations. The forward heaviest CP has now an average of 0.9 cm/ns, compared to 1.7 cm/ns for the data; the difference in velocity between the heaviest and the second heaviest CP is around 1 cm/ns, compared to 3 cm/ns for the data. This difference is due in part to higher energy thresholds for heavier ions. However, since the difference is three times larger, an important neck (intermediate velocity) contribution must be considered. Moreover, the panel (d) of the simulated distribution (figure 3) shows a depletion between the two backward-heaviest forward-heaviest contributions, in contrast with the experimental distribution. The presence of a faster and lighter PLE in the data and the formation of a neck-like structure at a velocity near the c.m. velocity would explain these differences.

The same beam at the same energy has been used on a natural Ta target to measure neutron energy spectra at different angles, in coincidence with charged particles yields. Neutron detectors were mounted at  $60^\circ$ ,  $90^\circ$ ,  $105^\circ$ , and  $150^\circ$  on one side of the scattering chamber and  $75^\circ$ ,  $90^\circ$ , and  $120^\circ$  on the other side, all in the same plane [9]. The quasi-projectile (QP) excitation energy distribution, determined by calorimetry from charged

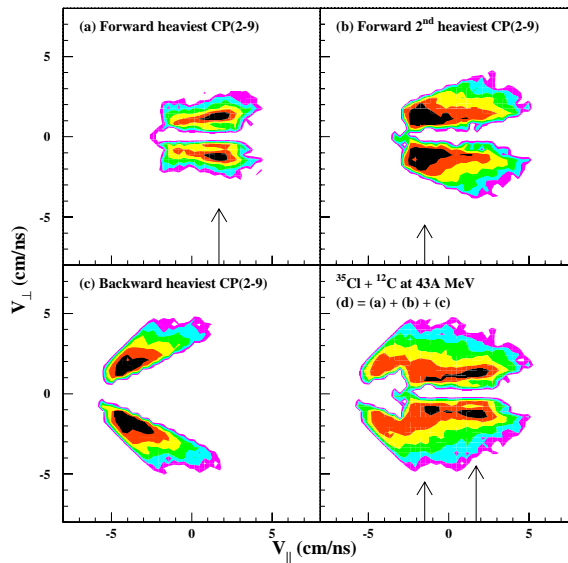


**Figure 2.** Galilean-invariant perpendicular versus parallel velocity spectra of charged particles ( $2 \leq Z \leq 9$ ) in the c.m. frame for the  $^{35}\text{Cl} + ^{12}\text{C}$  at 43 MeV/nucleon system with  $\Theta_{\text{flow}} < 45^\circ$  for the heaviest (top left) and second heaviest (top right) ions detected in the phoswich detectors and for the heaviest ions detected in the CsI(Tl) scintillators (bottom left). The total of the three distributions is shown in the bottom right panel. Parallel velocities are along the beam axis and the count yield is in a logarithmic scale. Arrows show the peak of the distributions for the heaviest and second heaviest charged particles.

particles of well defined peripheral events, has been divided in five bins. For each of them, the corresponding seven neutron energy spectra, taken in coincidence, were fitted simultaneously by a function representing the sum of two Maxwellian distributions, for two moving sources in the laboratory frame, the quasi-target (QT) and the midrapidity source (MRS). Surface emission has been assumed for calculations of the neutron energy spectra [10]. A QP source was not needed, since no neutrons from that source would be detected, except for a small contribution at  $60^\circ$ , as it has been shown from statistical simulations of a hot QP (8 MeV/nucleon excitation energy) performed with the code GEMINI [11]. The characteristics of the two emitting sources (QT and MRS), fixed by the fitting procedure, are displayed in figure 4, along with calculated values from the Boltzmann–Nordheim–Vlasov (BNV) code TWINGO [12]. They have been deduced from the measured neutron energy spectra taken in coincidence with well defined peripheral events: their evolution with the QP excitation energy shows new results. However, since that energy is always smaller than the one calculated from the QP velocity assumed for a pure dissipative binary collision, the missing excitation energy can be attributed to the MRS, experimentally evidenced from the neutron energy spectra. This, combined to the importance of the neutron multiplicity and the apparent temperature at midrapidity, emphasizes the importance of

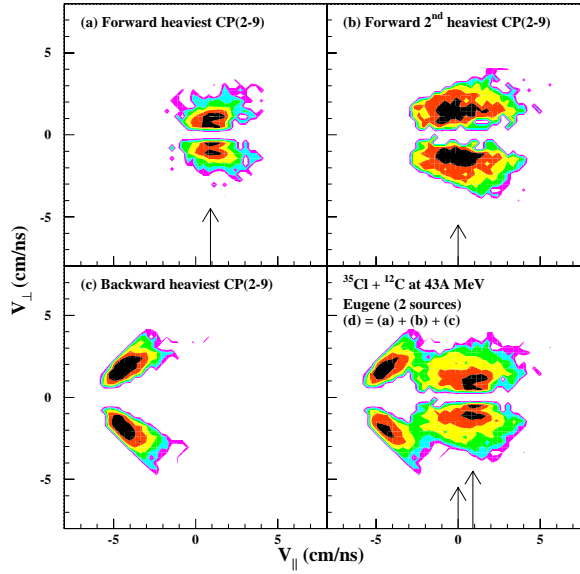


**Figure 3.** Same as figure 2 but for EUGENE two-source simulations of  $^{35}\text{Cl} + ^{12}\text{C}$  at 43 MeV/nucleon with  $b > 4.0$  fm and with  $\Theta_{\text{flow}} < 45^\circ$ .

pre-equilibrium and/or dynamical effects in the entrance channel. Finally, the MRS moves slower than the nucleon–nucleon c.m. velocity, showing that the attractive target mean field potential is still effective at 43 MeV/nucleon.

#### 4. Neck-like structure: Timescale and neutron asymmetry

Experimental evidence has been presented, above, for the existence of a neck-like structure, seen as a source moving at a velocity between the projectile velocity and the one expected for the target. Different properties of that structure or signs of its presence have been observed, like the apparent symmetrization occurring between the two collision partners [13], or its net tendency to emit neutron rich hydrogen isotopes [6]. By looking at the collision time-scale, it should be possible to deduce new information on the dynamics of the neck-like formation and the midrapidity emission. It is possible to extract IMF emission time by studying two-fragment correlation functions. Previous works [3] have been carried out on several reactions at different bombarding energies, but without an impact parameter neither a precise source selection. So, only averaged emission times over all sources have been extracted in general.

In the present analysis, IMF emission time has been deduced for well defined sources in the  $^{58}\text{Ni} + ^{197}\text{Au}$  reaction at 34.5 MeV/nucleon. It has been derived from the intensity-interferometry technique, based on two-fragment reduced-velocity correlation function, as following:

$$1 + R(V_{\text{red}}) = N_{\text{corr}}(V_{\text{red}})/N_{\text{uncorr}}(V_{\text{red}}), \quad (1)$$

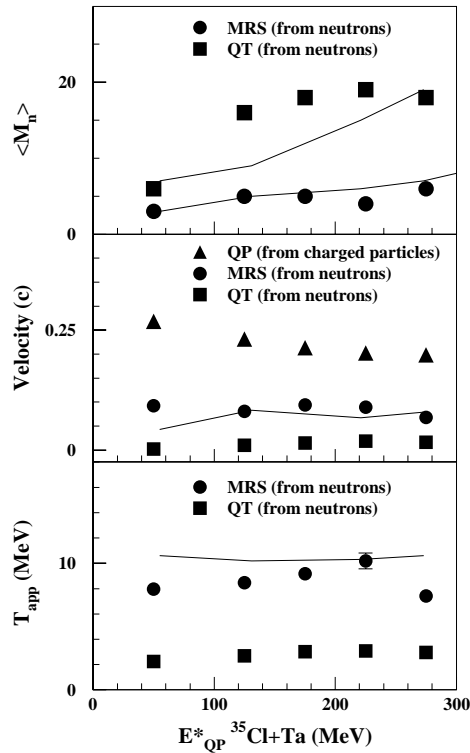


**Figure 4.** Average multiplicity of neutrons ( $\langle M_n \rangle$ ) emitted for the MRS and QT (top), source velocities (middle) and apparent temperature ( $T_{app}$ ) of neutron emitters versus  $E_{QP}^*$  (bottom) for the experimental data (dots) and dynamical BNV simulations for the MRS (lines). The error bars are from the MINUIT subroutines using multiparameter fits. When no error bar is present, the error is smaller than the size of the symbol.

with  $N_{corr}(V_{red})$ , the observed reduced-velocity distribution for fragment pairs selected from the same event and  $N_{uncorr}(V_{red})$ , the reduced-velocity distribution for fragment pairs selected from mixed events;  $V_{red} = |V_1 - V_2|/\sqrt{Z_1^2 + Z_2^2}$ .

Resulting two-fragment correlation functions, gated on the QP excitation energy, are shown in figure 5. The top panel is for fragments coming from the QP source and the bottom one, for fragments coming from MRS and QT source. Very few should come from the QT, because of high energy thresholds for IMF's. Two excitation energy bins only, one low and one high, are displayed (more complete results are given in [15]). For the QP source, yield suppression at low reduced velocity, due to the Coulomb interaction between the fragments, increases with excitation energy: a compact source emits fragments more quickly, for stronger Coulomb interactions between them than for a larger source which emits more slowly. Therefore, that yield suppression means an emission time-scale decreasing with excitation energy. In contrast, the MRS component shows little change from a low to a higher excitation energy, but shows a stronger Coulomb suppression at low reduced velocity, pointing out a shorter emission time than for the QP source. An emission time scale is extracted by comparing the data with simulations from the  $N$ -body Coulomb trajectory code of Glasmacher *et al* [16]. Hence, QP emission time decreases

with excitation energy from 2 to 6 MeV/nucleon, from 550 fm/c to 150 fm/c (see [15]). Above that energy, it becomes shorter and constant, indicating that multifragmentation might occur in the QP source. However, according to present results, it looks like the MRS component behaves in a way independent of impact parameter, or violence of the collision, at least for the class of events selected in the analysis.

Another analysis has allowed to understand more about the MRS. With three Si-Si-CsI(Tl) telescopes mounted in rings 2, 3, and 5 of the multidetector (see §2), providing isotopic resolution up to  $Z = 4$ , the reactions  $^{58}\text{Ni} + ^{12}\text{C}$  and  $^{24}\text{Mg}$  have been conducted at 34.5 MeV/nucleon. After dividing the collisions in three centrality classes (or according to their binary character), peripheral, midperipheral, and central collisions, on the flow angle criteria (see above), IMF isospin ratios ( $N/Z$ ) have been analysed in comparison to GEMINI [11] and SMM [18] simulations. Both codes are based on statistical decay assumptions, all particles and fragments being emitted simultaneously in SMM and sequentially, without Coulomb interaction, in GEMINI. The comparisons between simulations and experimental data are presented in figure 6 for the reaction  $^{58}\text{Ni} + ^{12}\text{C}$ . The behavior illustrated by those ratios supports the assumption of the formation and decay of a neutron-rich neck-like structure between the two main sources (QP and QT), even for the most central events generally described as a single source. That is consistent with the hypothesis already presented [4,9,13] about the important deformation of the two reaction partners inducing the formation of a neck zone between them.

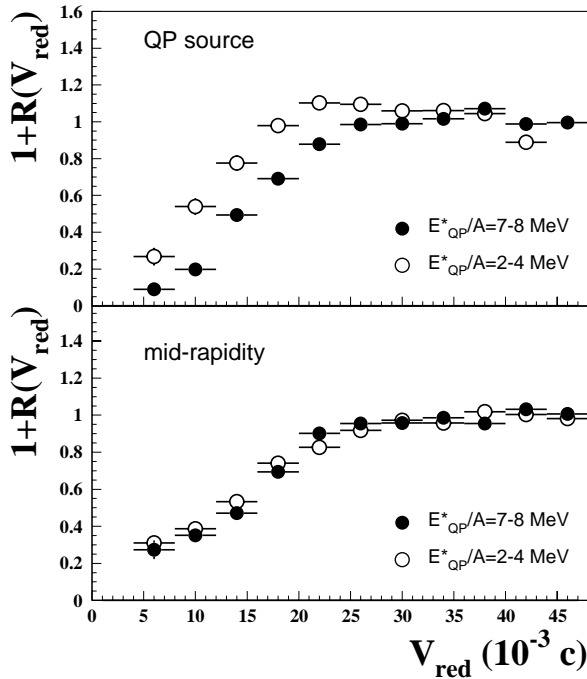


**Figure 5.** Correlation functions for quasi-projectile and midrapidity source in  $^{58}\text{Ni} + ^{197}\text{Au}$  system at 34.5 MeV/A, at low (empty circles) and high (full circles) excitation energy.

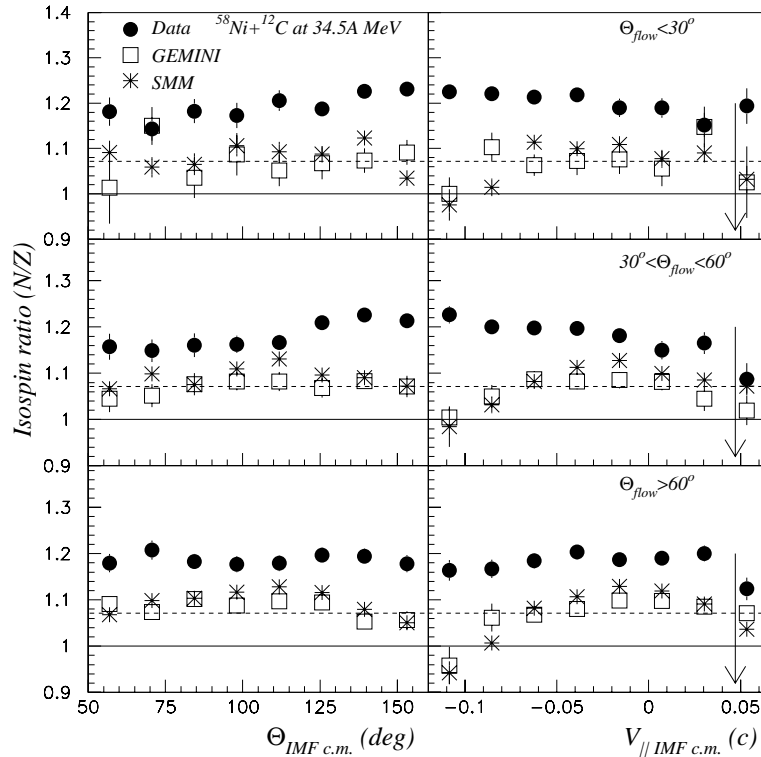


**Figure 6.** Average isospin ratios ( $N/Z$ ) for well identified IMF's with  $Z = 3$  or  $4$  as a function of the emission angle in the center of mass reference frame (left) and the center of mass particle velocity parallel to the beam axis (right) for the reaction  $^{58}\text{Ni} + ^{12}\text{C}$  at  $34.5A$  MeV (full dots). Cuts are made on  $\Theta_{flow} < 30^\circ$  (top),  $30^\circ < \Theta_{flow} < 60^\circ$  (middle) and  $\Theta_{flow} > 60^\circ$  (bottom). Open boxes represent filtered GEMINI simulations and stars are results from filtered SMM simulations (see text). Error bars are the statistical errors for a given angle or velocity bin. When no error bar is present, the error is smaller than the size of the symbol. The dotted lines show the isospin ratio for  $^{58}\text{Ni}$  (1.07) and the full line for  $^{12}\text{C}$  (1.00). The arrow shows the velocity of the  $^{58}\text{Ni}$  projectile in the center of mass frame for the  $^{58}\text{Ni} + ^{12}\text{C}$  reaction.

### 5. Conclusion

We have examined the formation of a neck-like structure in collisions between two heavy ions at intermediate energies. Various approaches of analysis have been applied on experimental data from several reactions measured with setups suited for charged particles and neutrons. Not only the results provide a solid ground to the existence of a neck zone, but they also support evidence for some of its properties. For instance, through the collision process, two nuclei tend to symmetrize; the process is fast, as shown by the IMF correlation functions, and its time-scale does not seem to be correlated to the QP excitation energy. Neutron rich light particles are preferably emitted by the midrapidity region, as the

IMF's coming from the same zone exhibit a neutron richness larger than the two original nuclei. Results are leading towards a common and general observation, the importance of dynamics in heavy ion collisions.

### **Acknowledgments**

We would like to thank our collaborators from Chalk River Laboratories and A S Botvina, R J Charity, D Durand and T Glasmacher for the use of their codes. This work has been supported in part by the Natural Sciences and Engineering Research Council of Canada and the Fonds pour la Formation de Chercheurs et l'Aide à la Recherche du Québec.

### **References**

- [1] L G Moretto and G J Wozniak, *Ann Rev. Nucl. Part. Sci.* **43**, 379 (1993) and references therein
- [2] J Pochodzalla *et al*, *Phys. Rev. Lett.* **75**, 1040 (1995)
- [3] D Durand, *Nucl. Phys.* **A630**, 52c (1998)
- [4] L Gingras *et al*, *XXXVI International Winter Meeting on Nuclear Physics* (Bormio, Italy, 1998) p. 365
- [5] C P Montaya *et al*, *Phys. Rev. Lett.* **73**, 3070 (1994)  
J Toke, *et al*, *Phys. Rev. Lett.* **75**, 2920 (1995)  
J F Lecolley *et al*, *Phys. Lett.* **B354**, 202 (1995)
- [6] Y Larochelle *et al*, *Phys. Rev.* **C55**, 1869 (1997)
- [7] J Cugnon and D L'Hote, *Nucl. Phys.* **A397**, 519 (1983)
- [8] D Durand, *Nucl. Phys.* **A541**, 266 (1992)
- [9] Y Larochelle *et al*, *Phys. Rev.* **C59**, R565 (1999)
- [10] R Wada *et al*, *Phys. Rev.* **C39**, 497 (1989)
- [11] R J Charity *et al*, *Nucl. Phys.* **A483**, 371 (1988)
- [12] A Guarnera, Ph D. thesis (University of Caen, France, 1996)  
M Colonna *et al*, *Nucl. Phys.* **A541**, 295 (1992)
- [13] Y Larochelle *et al*, *Phys. Rev.* **C57**, R1027 (1998)
- [14] D R Bowman *et al*, *Phys. Rev. Lett.* **70**, 3534 (1993); *Phys. Rev.* **C52**, 818 (1995) and references therein
- [15] Zhi-Yong He *et al*, *Phys. Rev.* **C63**, 011601-1 (2000)
- [16] T Glasmacher *et al*, *Phys. Rev.* **C50**, 952 (1994)
- [17] Y Larochelle *et al*, *Phys. Rev.* **C62**, 051602-1 (2000)
- [18] A S Botvina *et al*, *Nucl. Phys.* **A507**, 649 (1990) and references therein